Electronic Supplementary Material (ESI) for RSC Advances.

Supplementary Information for

A high-performance transparent graphene/vertically aligned carbon nanotube (VACNT) hybrid electrode for neural interfacing

Du Won Jeong,[a†] *Gook Hwa Kim,*[b†] *Na Yeon Kim,*[c] *Zonghoon Lee,*[c] *Sang Don Jung*[b*] *and Jeong-O Lee*[a*]

[a]Dr. Du Won Jeong and Dr. Jeong-O Lee
Advanced Materials Division, Korea Research Institute of Chemical Technology (KRICT), 141 Gajeong-ro, Yuseong-gu, Daejeon 34114, Korea

[b]Gook-Hwa Kim and Dr. Sang-Don Jung
Synapse Device Creative Research Section, Electronics and Telecommunications Research Institute (ETRI), 218 Gajeong-ro, Yuseong-gu, Daejeon 34129, Korea

[c]School of Materials Science and Engineering, Ulsan National Institute of Science and Technology (UNIST), 50 UNIST-gil, Ulsan 44919, Korea

[†]These authors contributed equally to this work.

[*]E-mail: jungpol@etri.re.kr, jolee@krict.re.kr

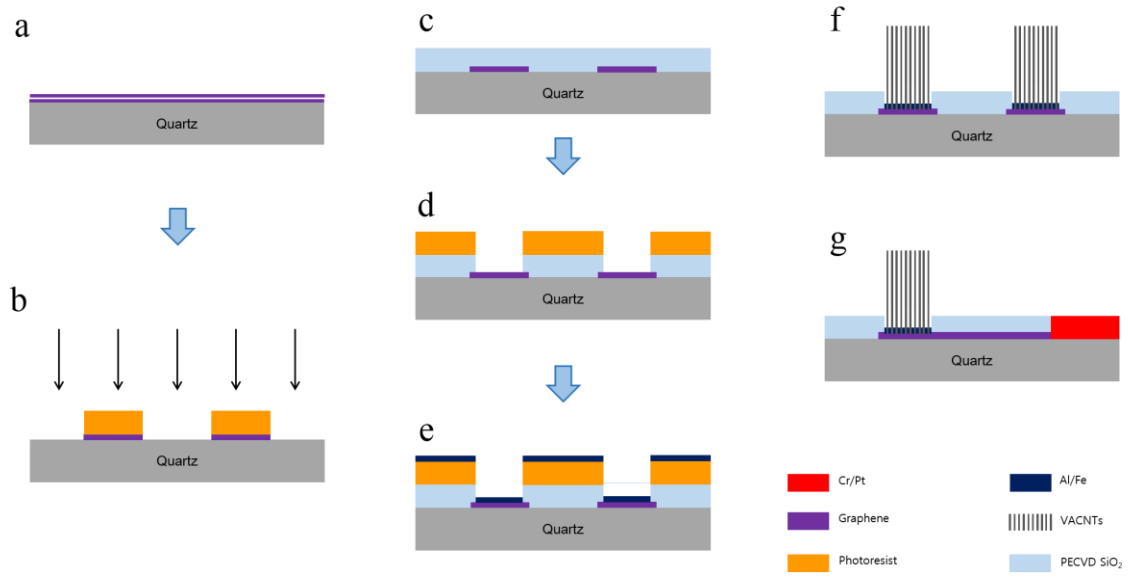

Fig. S1 Process of fabricating the TGVH device. (a) two-layer graphene was transferred onto the Cr/Pt (5/30 nm) electrodes patterned using photolithography and sputtering deposition. (b) The photoresist that served as a mask was patterned along with the Pt electrodes using photolithography. The patterned two-layer graphene was then etched with oxygen plasma over 20 min. (c) A passivation layer (500 nm SiO_2) was deposited using the PECVD method. (d) Five micrometer windows were opened using wet etching to obtain (e) the patterned catalyst (8/1–3 nm = Al/Fe). (f) TGVH electrodes with a 6 × 6 array of internal Pt ground electrodes and inter-electrode distances of 200 μm were grown using low-pressure PECVD at 650°C for 12 min. (g) Another view of a TGVH device.

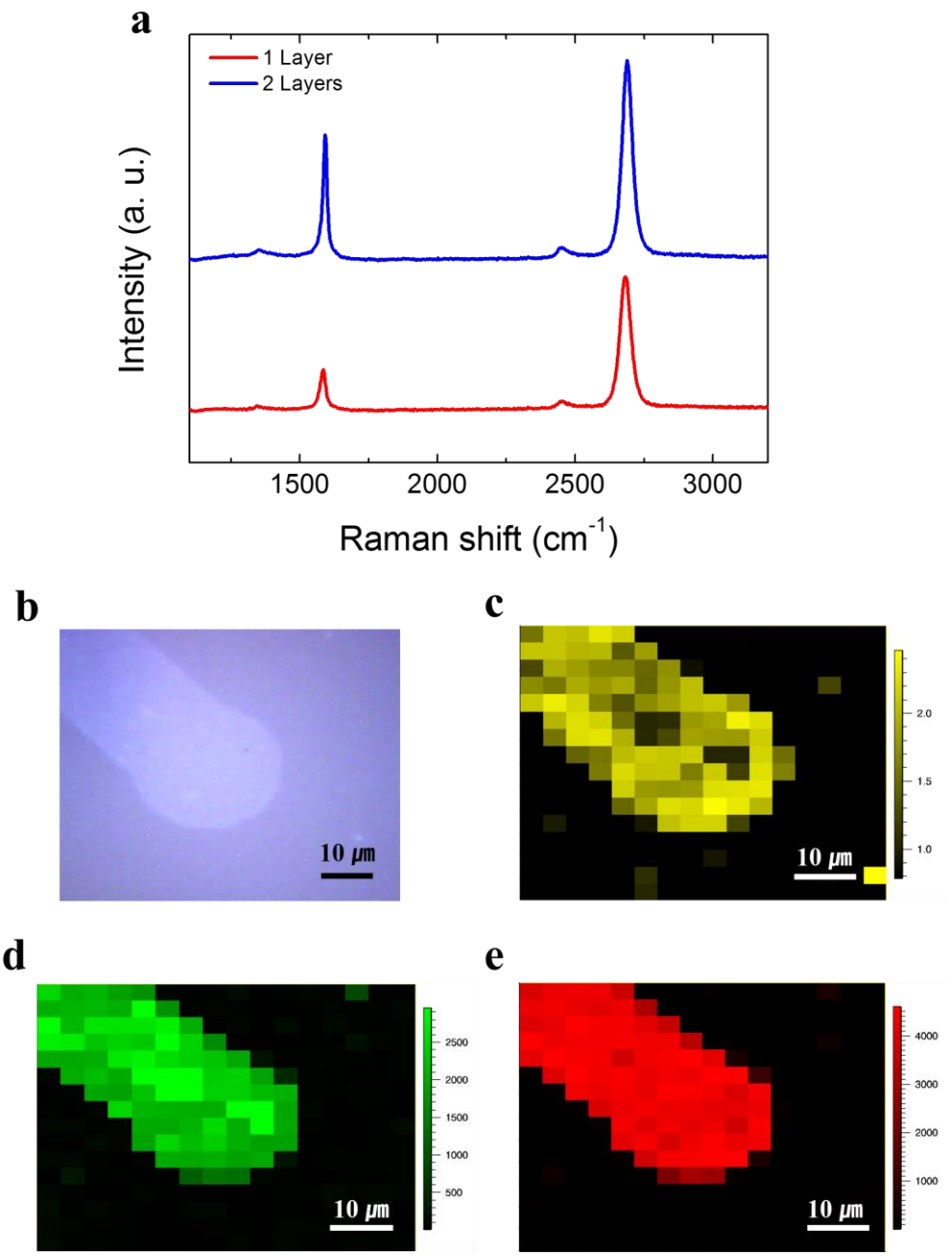

Fig. S2 Raman spectra of a graphene electrode. (a) Raman spectra of single- and two-layer graphene. The 2D peaks obtained from the single- and two-layer graphene corresponding to 2682 cm^{-1} and 2689 cm^{-1}, respectively. The G peaks obtained from the single- and two-layer graphene were 1584 cm^{-1} and 1592 cm^{-1}, respectively. Both samples exhibited weak D peak intensities. (b) Optical image of a patterned two-layer graphene electrode. (c) Raman spectral mapping of the 2D/G peak ratio, (d) G peak, and (e) 2D peak.

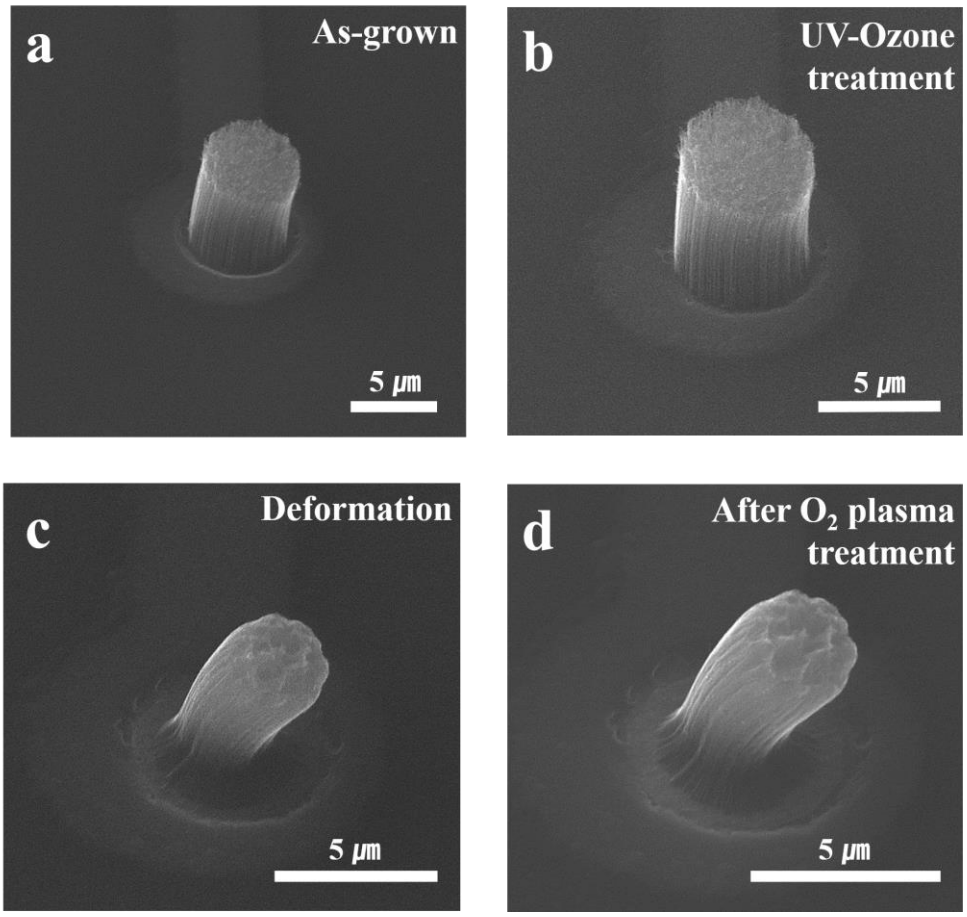

Fig. S3 VACNT electrode deformation process. (a) As-grown VACNT electrode. (b) The VACNT electrode was functionalized under UV-ozone treatment over 20 min. (c) VACNT electrode with a deformed structure as a result of dipping in DI water over 10 min. (d) The modified VACNT electrode with a nano-scale surface underwent O_2 plasma treatment for 5 min to coat the electrode surface with a PDL layer that enhanced adhesion between the cells and the graphene-VACNT device.

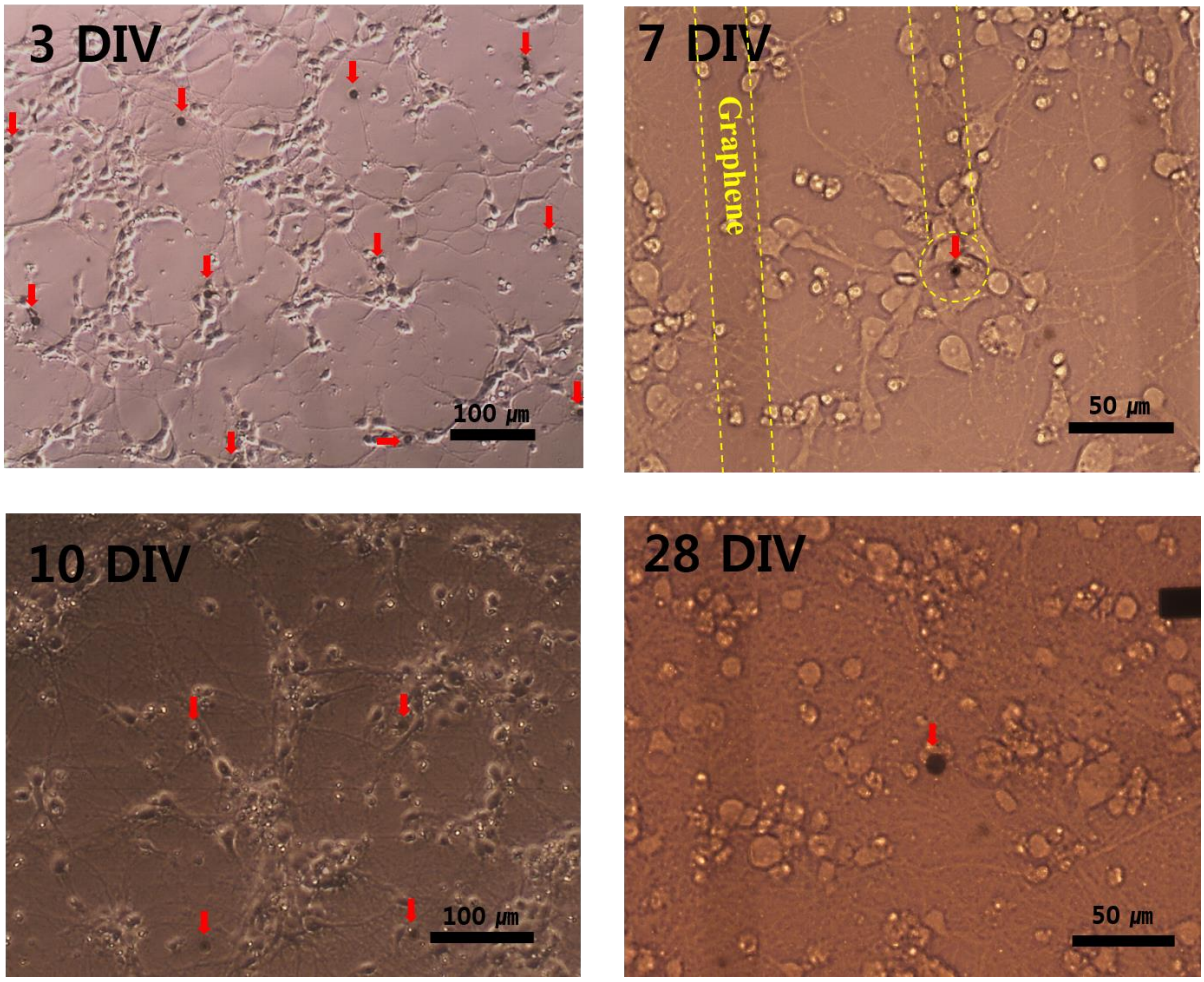

Fig. S4 Optical images of cortical neurons cultured on a TGVH device at 3–28 DIV (the red arrows and the area highlighted by a yellow dashed line correspond to the VACNT electrodes and graphene, respectively).

Home-built MEA System for recording the neuronal signals

An MEA system was designed for neuronal signal recording. This system included measurement and temperature control systems, as shown in Fig. S5 (a). Signals in 64 channels could be recorded concurrently. Fig. S5(b) illustrates the signal measurement process, consisting of 4 steps: AC coupling, buffering, amplifying, and low-pass filtering. The signals from the cells were sent to an AC coupler (a passive high pass filter served as a filter beyond 0.1 Hz), and then to a buffer (the impedance was reduced to remove interference between the electrode and the measuring system). Signals that underwent this two-step process were amplified by a factor of 1,000 and then filtered below 10 kHz. These signals were collected using a USB-6255 (NI, DAQ), and digitalized. During the experiments, the bottom of the MEA was maintained at 37°C using a hot plate.

Our system was compared with a commercial Multi Channel System (MCS) by recording signals generated by a signal generator (SG, made by MCS) using the MCS and MEA systems. Fig. S5(c, d) presents signals recorded using the MCS and MEA systems, respectively. The amplitudes of the spikes were similar, whereas the RMS noise in the MCS and MEA systems were 1.47 μV and 0.87 μV, respectively. The RMS noise (n= 5000) was calculated according to

$$V_{noise} = \sqrt{\frac{1}{n}\sum_{i=0}^{n-1}|V_i|^2}, \quad \text{(Eq. 1)}$$

where n is the number of samples, V_i is the voltage amplitude.

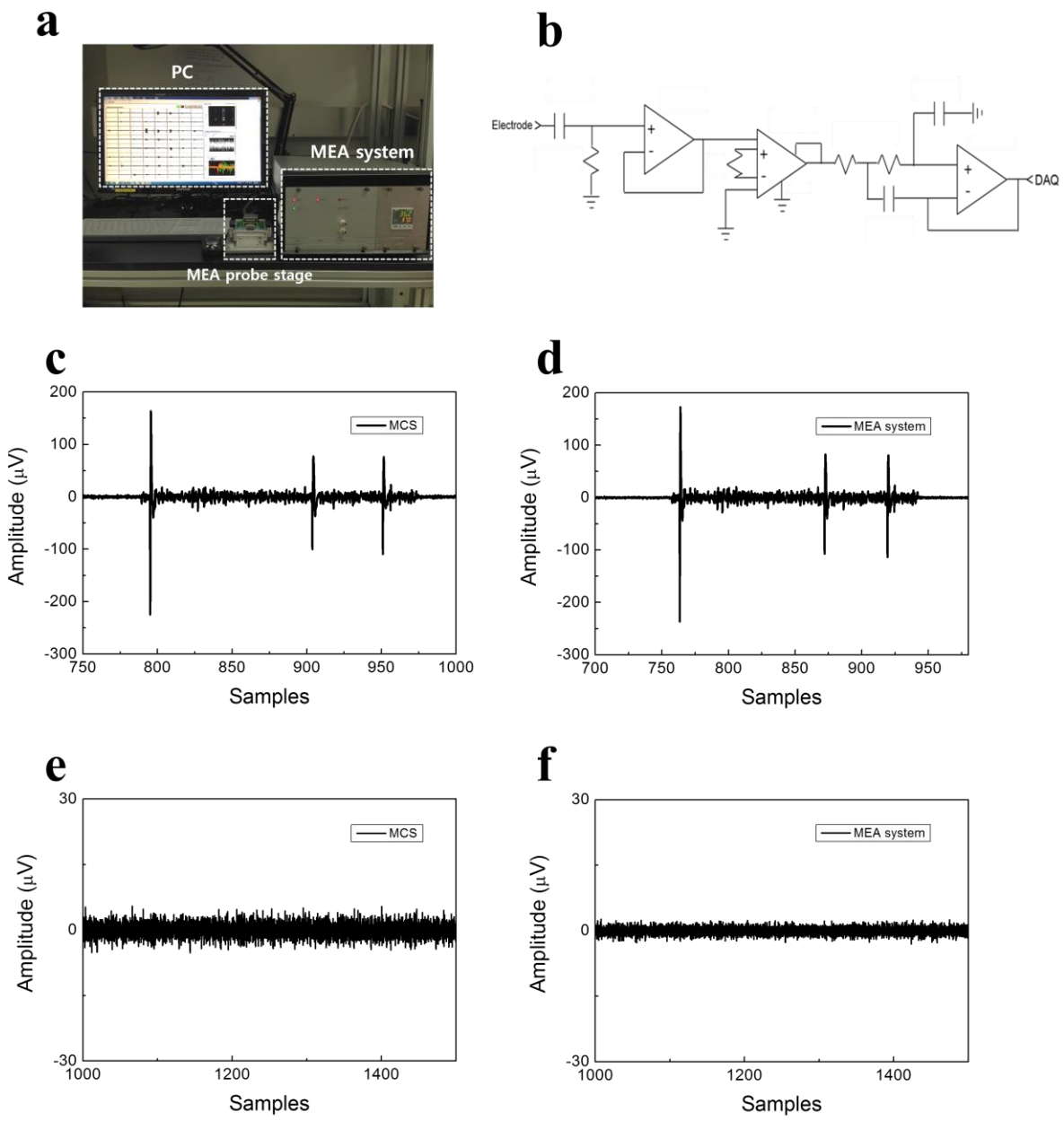

Fig. S5 Home-built MEA system. (a) Configuration of the MEA system for recording neuronal cell signals. (b) Block diagrams of a single-unit recording circuit, including an amplifier and a band pass filter. (c) The MCS and (d) MEA systems corresponding to the signals recorded from the SG device. SG recording noise obtained using the (e) MCS or (f) MEA.

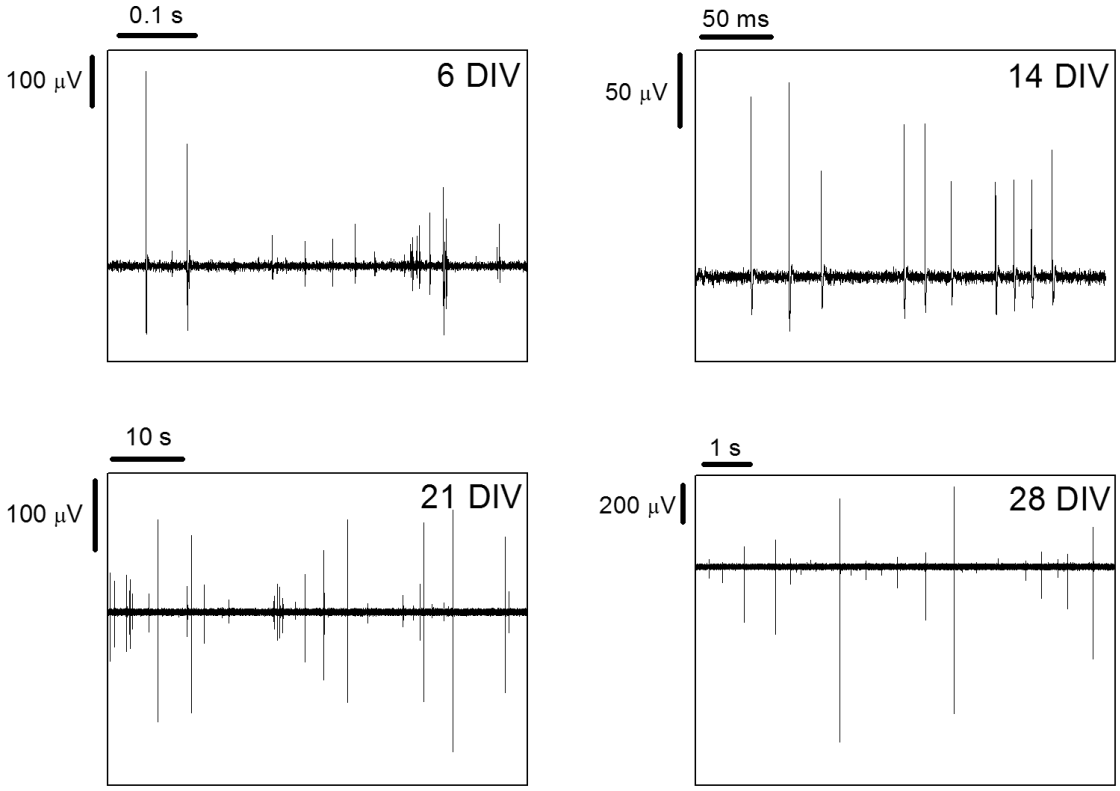

Fig. S6 Extracellular action potential signals recorded from cortical neurons cultured on a TGVH device, 6–28 DIV.

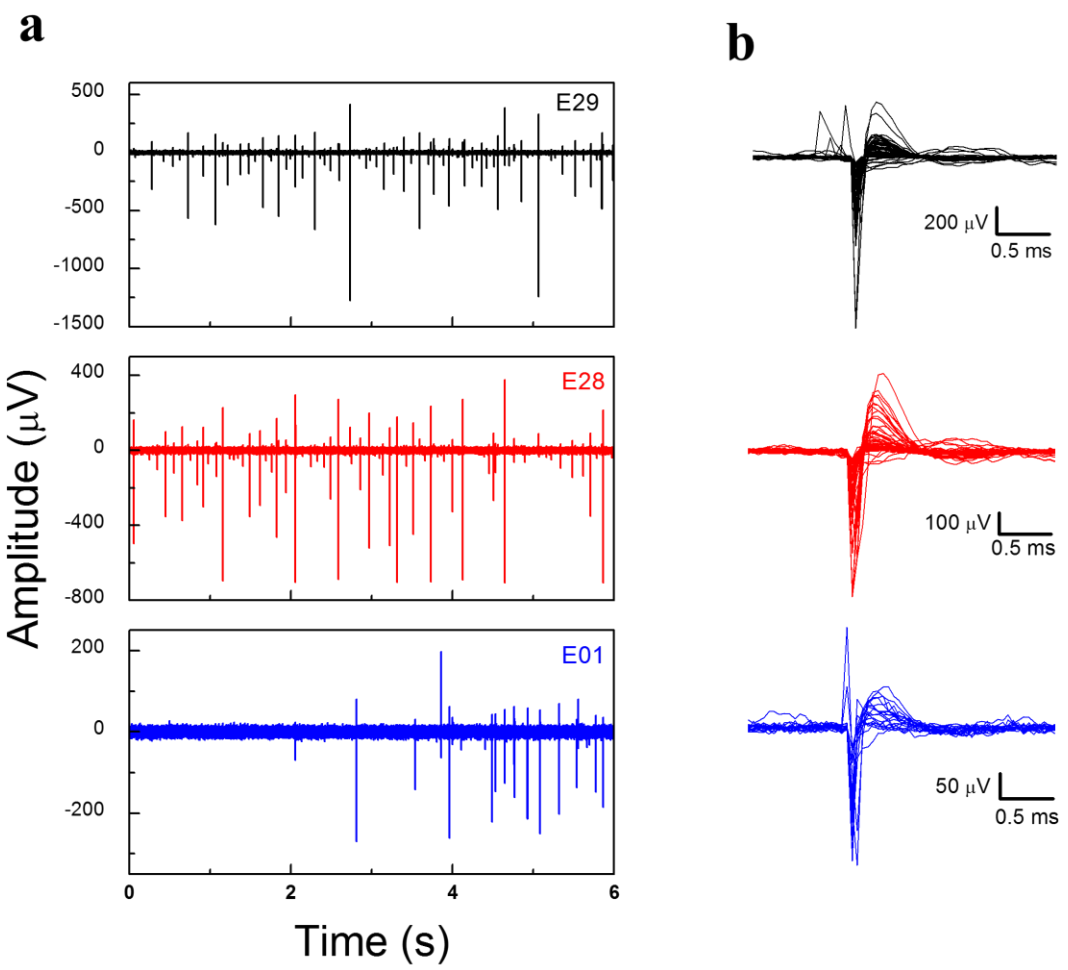

Fig. S7 (a) Spontaneous cortical neuron action potentials with a threshold voltage of –25 μV, measured using three representative electrodes at 7 DIV. In E29, the maximum peak-to-peak amplitude was 1.6 mV, the signal-to-noise ratio (SNR) of which was approximately 270. (b) The sorted spikes collected from each electrode over 3 ms.

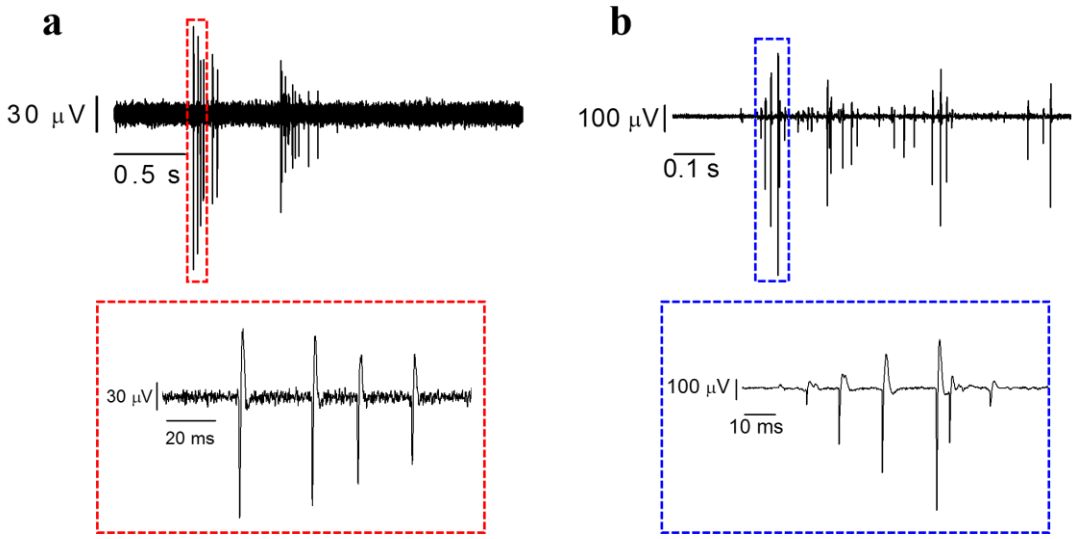

Fig. S8 Partial burst firing activity of the neuron cells. Signals recorded from the VACNTs electrode at (a) 21 DIV and (b) 27 DIV.

The distance dependence of the spike amplitude

Superposition of multi-unit spikes recorded using a single electrode (E29 in Fig. S7(a)), except for the plus phase, were sorted over a range of amplitudes. Fig. S9(a) plots all recorded signals, sorted into 8-type single-unit spikes, as shown in Fig. S9(c). The distribution of spike amplitudes with a threshold of –25 μV, measured using the E29 electrode, is shown in Fig. S9(b). The spike amplitude decreased according to

$$\Phi(\mathrm{d}) = \frac{1}{2\pi\sigma}\left(\frac{\mathrm{I}}{\mathrm{d}}\right), \qquad \text{(Eq. 2)}$$

where Φ is the potential obtained from the point–current source (I) located at a distance (d) within the medium, with a conductivity of (σ), considering a point source. The number of cells (n) around each electrode in a two-dimensional circle could be described as

$$\mathrm{n} = \mathrm{C} \cdot \pi r^2, \qquad \text{(Eq. 3)}$$

where C is a proportionality constant, r is the radius. If the radius is equal to the distance (d), the number of spikes was closely related to the number of cells present. The detected spike average amplitude relationship then became

$$\mathrm{n} = \frac{A}{\Phi^2}, \qquad \text{(Eq. 4)}$$

where A is constant. The number of detected spikes was closely related to the amplitude of the recorded spikes, as determined by the fitting constant B in Fig. S(b).

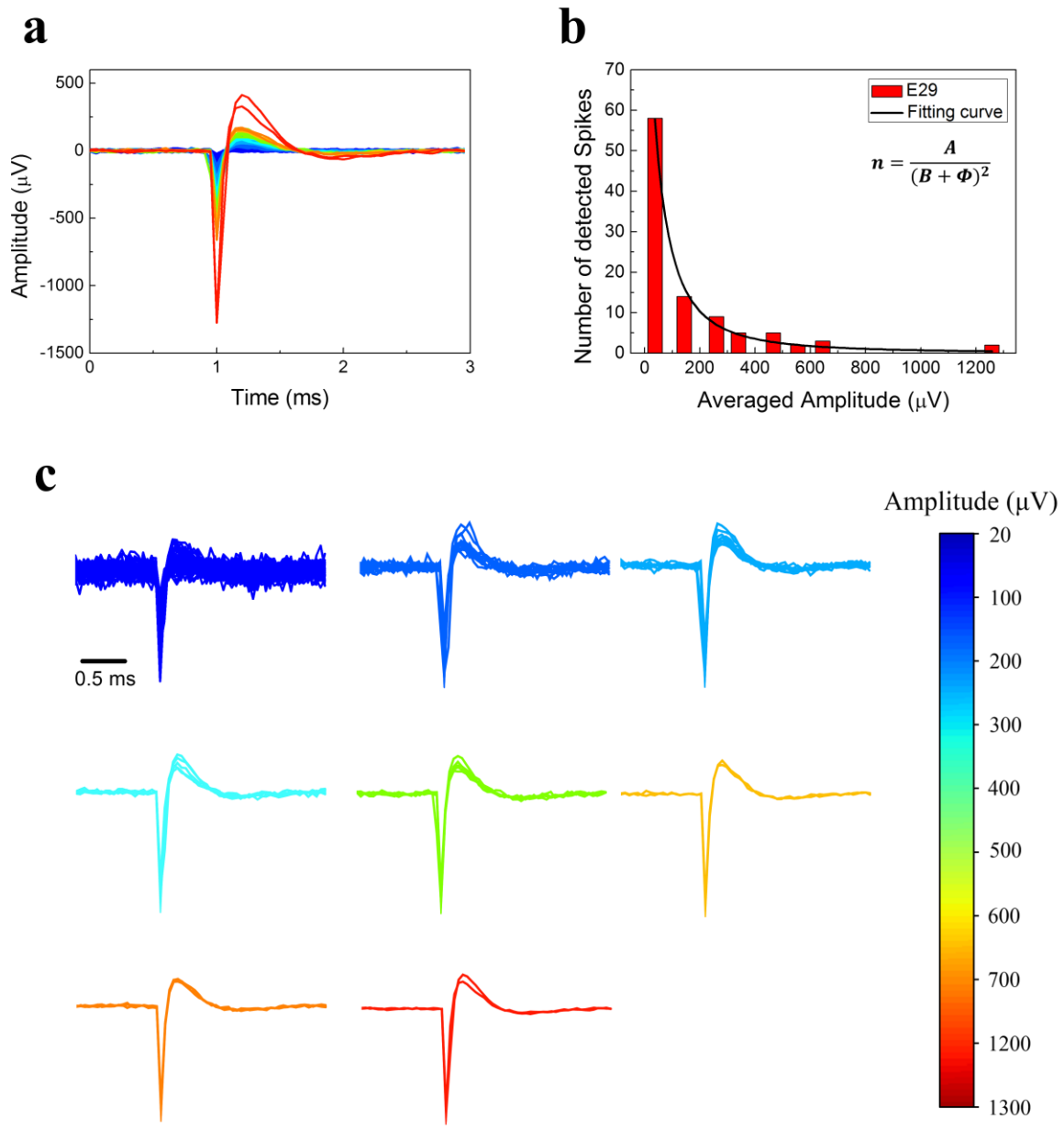

Fig. S9 The distribution of the number of detected spikes and the average spike amplitude. (a) The superposition of multi-unit spikes given a –25 μV threshold, recorded using a single electrode (E29 in Fig. S8), with the exception of the positive-phase spikes. (b) Distribution of the number of detected spikes as a function of the average amplitudes, based on (c) and sorted into 8 types of single-unit spike over a range of amplitudes.

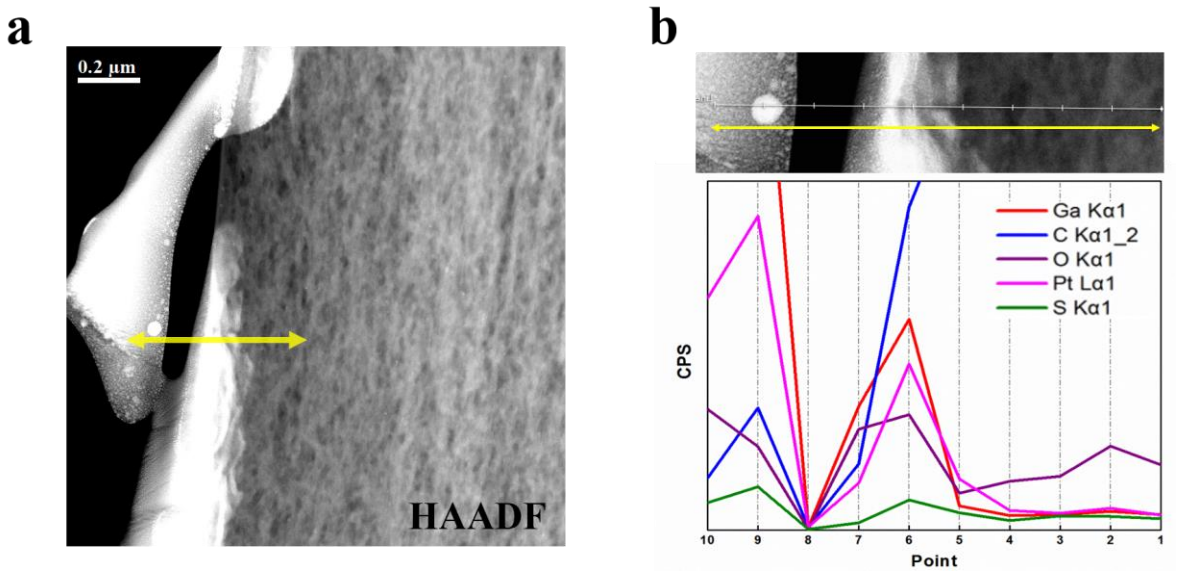

Fig. S10 TEM analysis of the interface between the VACNT electrode and the cell. (a) High-angle annular dark-field (HAADF) image. (b) The EDS results revealed that the S distribution was only detected in the area around the cell membrane.

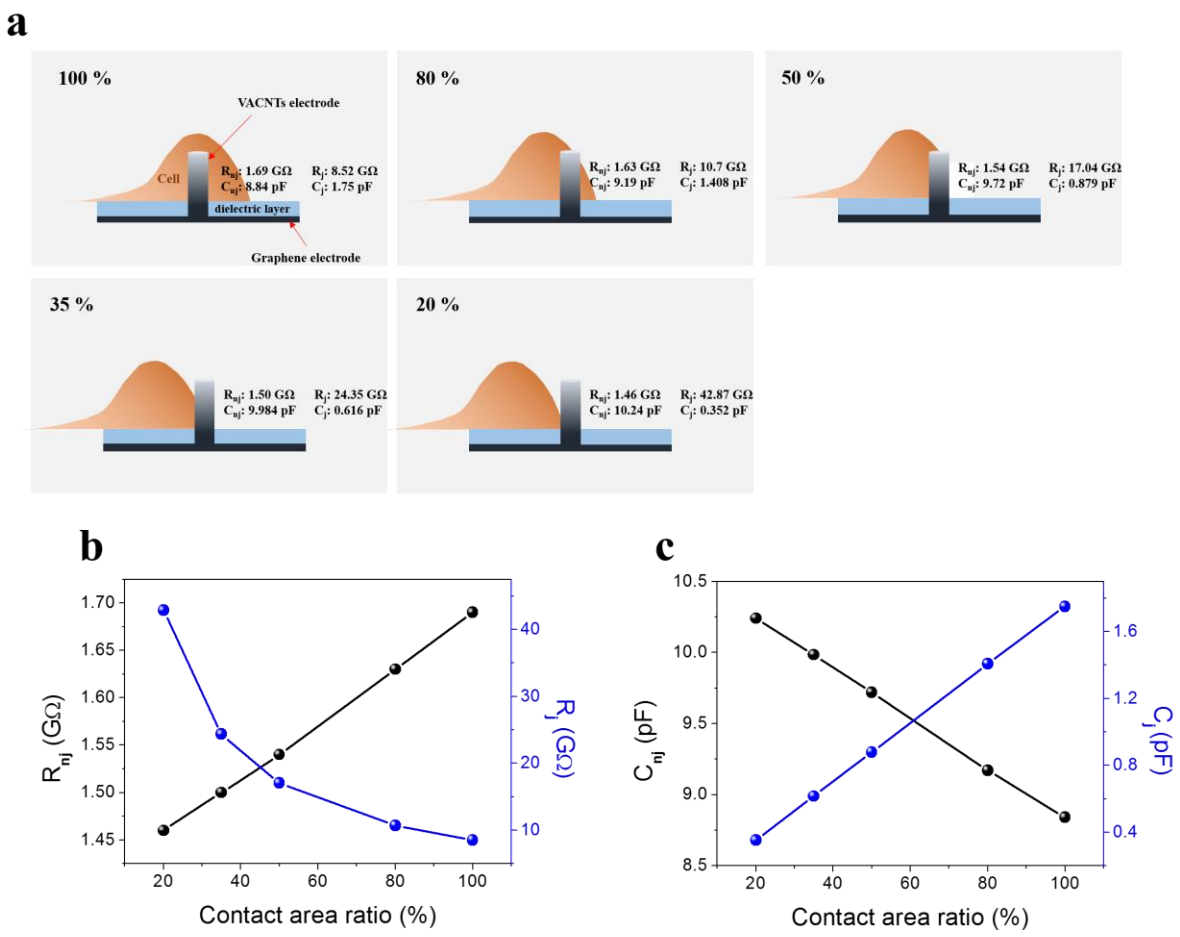

Fig. S11 (a) Schematic diagram of the contact ratio between the VACNTs and a neuronal cell, over the range 100–20%. (b) Resistance values of the non-junction and junction; (c) Capacitance values of the non-junction and junction varied as a function of the contact ratio.

Simulation of the extracellular action potential

The interface between a neuron and a VACNT electrode was characterized by designing an equivalent circuit model based on the impedance spectroscopy and parameters of the measurement system. This model was used to simulate the signals recorded from the VACNT electrodes. The extracellular action potentials recorded from neurons were simulated using OrCAD PSpice, where the model of the neuron was used by Hodgkin & Huxley[1] and the action potential was generated by a current pulse (amplitude: 7 μA/cm^2, duration: 0.2 ms).[2] The diameter of the soma of a primary cortical neuron was estimated to be approximately 10 μm, assuming that a neuron is a sphere. The surface area was assumed to be 1,062 μm^2. The surface of a VACNT electrode was calculated to be 176 μm^2 (considered to be a cylinder). The capacitance (C_m) and resistance (R_m) of a neuron membrane were 1 μF/cm^2 and 15 kΩ·cm^2, respectively.[3,4]

In this neuron model, the total membrane capacitance (C_m) was taken to be 10.6 pF, according to the surface area of a neuron, and the membrane resistance (R_m) was defined as 1.415 GΩ. The surface area of a neuron was divided into a junctional membrane that faced the electrode and a non-junctional membrane that faced the bathing solution and the substrate.[5] The membrane parameters of the junction and non-junction depended on the area ratio of the junction (k_j) and non-junction (k_{nj}) with the VACNT electrode, respectively.[6,7]

The non-junction area ratio was calculated using Eq. 5:

$$k_{nj} = \frac{A_{cell} - kA_e}{A_{cell}}. \quad \text{(Eq. 5)}$$

The junction area ratio was calculated using Eq. 6:

$$k_j = \frac{kA_e}{A_{cell}}, \quad \text{(Eq. 6)}$$

where A_{cell} and A_e correspond, respectively, to the entire surface area of a neuron and the surface area of an electrode, and k is the junction ratio. The capacitances of a junction (C_j) and a non-junction (C_{nj}) could be written as $C_m \cdot k_j$ and $C_m \cdot k_{nj}$, respectively. The resistance of a junction (R_j) and a non-junction (R_{nj}) could also be written as R_m/k_j and R_m/k_{nj}, respectively. The seal resistance was determined by the distance between the cell and the electrode/junction coefficient. The simulation model parameters are listed in Table S1.

Fig. S12(a) plots sorted spikes obtained from a representative VACNT electrode and analyzed using PCA, as shown in Fig. S12(b). These spikes include three types of clusters (Fig. S12(c)). One such type (green line) was again classified into two types of clusters with different amplitudes using a PCA analysis, as shown in Fig. S12(d). The sorted spikes (gray line, n=19) were used as objects in the simulations, the average spike of which is given by the black line with a –632 μV maximum amplitude, as shown in Fig. S12(e). The simulated spike corresponded roughly to the average spike, given a 35% contact ratio (Fig. S12(a), based on the parameters presented in Fig. S12(b)), with a 50 MΩ seal resistance.

Table S1. List of simulation parameters.

Model parameters	Symbol	Values	Units
Resistance of the cell membrane	R_m	1.415	GΩ
Capacitance of the cell membrane	C_m	10.6	pF
Leakage resistance	R_L	51.9	kΩ
Mass capacitance	C_L	13.17	pF
Warburg element	Z_w	8.11	MΩ
Resistance between electrode and electrolyte	R_{ct}	1.57	MΩ
Equivalent series resistance	R_s	2.7	kΩ
Double layer capacitance	CPE_{dl}	1.164	nF
Resistance of measurement system	R_{sys}	10	MΩ
Capacitance of measurement system	C_{sys}	90	pF
Seal resistance	R_{seal}	1–100	MΩ

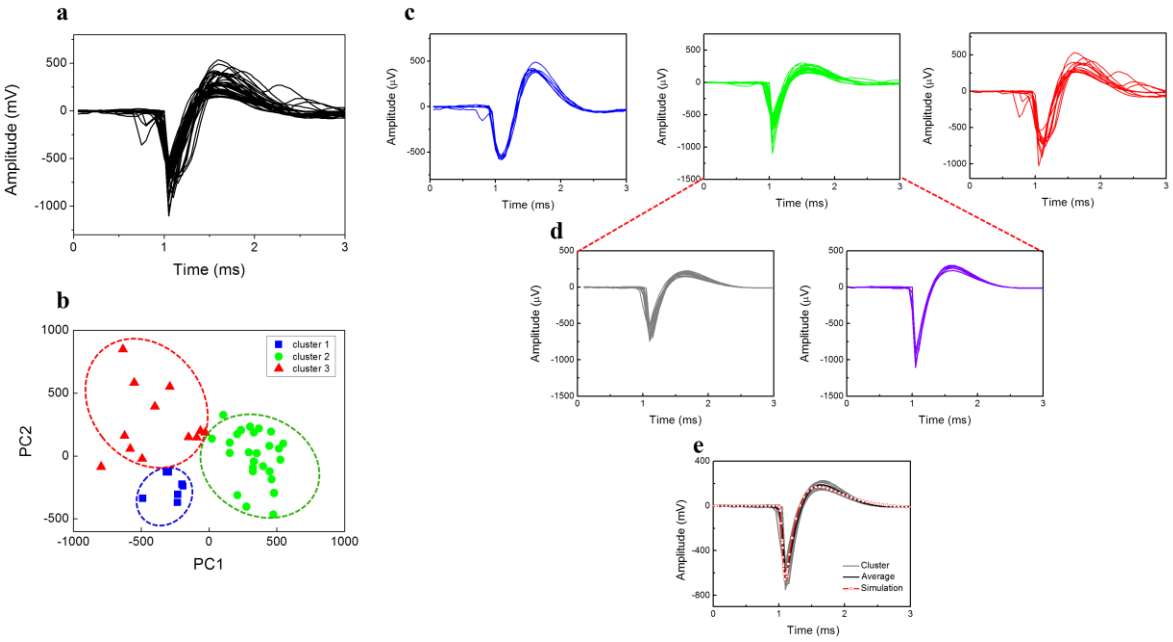

Fig. S12 (a) Sorted spikes, collected over 5 min of recordings at a –600 μV threshold voltage from a single VACNT electrode (E21) at 27 DIV. (b) The PCA results classified clusters according to (c) 3 types using the machine learning toolkit (LabVIEW). (d) One of the clusters (green line) was further classified into two types based on the spike amplitude. (e) The gray line of the cluster was used in the simulation, and the black line of the cluster indicated the average cluster. The red line represents the simulated action potential.

References

1 A. L. Hodgkin, A. F. Huxley, *J. Physiol.* 1952, **117,** 500–544.

2 S. Martinoia, P. Massobrio, *Biosensors and Bioelectronics* 2004, 19, 1487–1496.

3 C. Koch, *Biophysics of computation: information processing in single neurons,* Oxford University Press, New York, 1999

4 N. Spruston, D. Johnston, *J. Neurophysiol.* 1992, **67,** 508–529.

5 U. Ashery, R. Penner, M. E. Spira, *Neuron* 1996, **16,** 641–651.

6 M. E. Spira, A. Hai, *Nat. Nanotechnol.* 2013, **8,** 83–94.

7 A. Hai, J. Shappir, M. E. Spira, *J Neurophysiol.* 2010, **104,** 559–568.